Response of a Simplified Oceanic General Circulation Model to Idealized NAO-like Stochastic Forcing

C. HERBAUT, J. SIRVEN, AND S. FÉVRIER

Laboratoire d'Océanographie Dynamique et de Climatologie, UMR/CNRS/ORSTOM/Université Pierre et Marie Curie, Paris, France

(Manuscript received 23 August 2001, in final form 2 May 2002)

ABSTRACT

The response of a simplified model of the subtropical and subpolar gyres to a mechanical stochastic forcing that mimics the North Atlantic Oscillation (NAO) is studied. An internal damped mode of oscillation with a 22–24-yr period is found, with a maximum amplitude in the northwestern part of the basin (subpolar gyre and intergyre area). Its mechanism is as follows. In response to the wind stress forcing, anomalous currents appear between 35° and 40°N. They create temperature anomalies near the western coast, which are in turn advected by the mean current into the subpolar gyre and in the convection area. These temperature anomalies affect the thermohaline circulation, which produces new temperature anomalies near 35°–40°N and thus appears as a key component of this damped periodic mode. Wind stress forcing acts as efficiently as heat flux at exciting this oscillation, which can persist if external forcing is strong enough.

1. Introduction

Decadal and interdecadal variations of sea surface temperature (SST) over the North Atlantic have been documented in the observations (Deser and Blackmon 1993; Hansen and Bezdek 1996; Sutton and Allen 1997) and have been shown to be partly related to fluctuations of the North Atlantic Oscillation (hereinafter NAO), the dominant mode of variability of the atmosphere over the North Atlantic (Kushnir 1994). Whether they reflect a passive response of the ocean to the atmospheric forcing or they reflect active two-way interactions between the two media is not well established.

On the one hand, Frankignoul et al. (1997) have shown that a passive response of the ocean interior to stochastic wind stress forcing suffices to lead to decadal variability. Jin (1997) also established that a weak peak in the power spectrum of the meridional heat transport appears at decadal to interdecadal timescale when the ocean is forced by a stochastic wind stress with an organized stationary spatial stucture. Using a model forced by a harmonic forcing and National Centers for Environmental Prediction–National Center for Atmospheric Research (NCEP–NCAR) reanalyses, Krahmann et al. (2001) showed that the wind stress pattern characteristic of the NAO could form SST anomalies off the east coast of North America, which are then advected along the North Atlantic Current. They suggested that the mechanism at work in their model is in agreement with the one-dimensional stochastic model of Saravanan and McWilliams (1998). In this simple model, a spatially coherent atmosphere can enhance the response of an advective ocean at preferred timescale. On the other hand, using a fully coupled model, Grötzner et al. (1998) suggested that the decadal variability over the North Atlantic could arise from a coupled mode including the NAO. In an analytical study, Marshall et al. (2001) similarly proposed a coupled mechanism involving the NAO wind stress: wind stress anomalies force large heat transport anomalies between the gyres, which in turn could affect the atmosphere.

Here, we extend the work of Krahmann et al. (2001) by studying the response of an idealized ocean basin to stochastic NAO-like wind stress forcing. In positive phases of the NAO, the westerlies are intensified, and the oceanic heat loss strengthens over the subpolar gyre while the subtropical gyre gains more heat (Cayan 1992). The reverse occurs during negative phases. Our study is limited to the decadal oceanic response to these large-scale wind stress and heat fluxes anomalies; we do not consider changes associated with smaller spatial scale or shorter timescale. We focus on the dynamics of the region between the subtropical and subpolar basins (hereinafter called the intergyre region) and on the thermohaline response. We begin in section 2 with a brief description of the model and the numerical experiments that have been performed. In section 3, the main results are described and a mechanism that explains them is proposed. In section 4, sensitivity ex-

Corresponding author address: Christophe Herbaut, Laboratoire d'Océanographie Dynamique et de Climatologie, Université Pierre et Marie Curie, T14, étage 2, CC100, 4 place Jussieu, Paris 75252, Cedex 5, France.
E-mail: ch@lodyc.jussieu.fr

periments are presented. Discussion and conclusions are given in section 5.

2. Model setup and numerical experiments

We used the Massachusetts Institute of Technology primitive equation model (Marshall et al. 1997), which was limited to an idealized basin of constant depth $H = 4000$ m on a sphere that extends from the equator to 60°N and from 60°W to 0°. The horizontal resolution is 1° × 1°. There are 10 levels in the vertical, with 5 in the upper 600 m. The equation of state of seawater has the simplified form,

$$\rho = \rho_0[1 - \epsilon(T - T_0)],$$

where ϵ is a coefficient of thermal expansion ($\epsilon = 2 \times 10^{-4}$ K^{-1}), ρ_0 is a mean density ($\rho_0 = 10^3$ kg m^{-3}), and T_0 is a reference temperature profile. The influence of salinity is not considered. The horizontal eddy viscosity and thermal diffusivity are respectively equal to 10^4 and 10^3 m^2 s^{-1}. The vertical viscosity and diffusivity are respectively equal to 10^{-3} and 10^{-4} m^2 s^{-1}, as in Cox (1985). Convection is parameterized by a nonpenetrative convective adjustment scheme when static instability occurs. No-slip boundary conditions are used.

By using an accelerating convergence method (Bryan 1984), the model has been spun up from rest for 540 yr, whereupon a steady-state solution (hereinafter referred to as the reference state) is achieved in the upper 1000 m. The wind used for this spinup (Figs. 1a,b) varies both zonally and meridionally, so that the observed tilt from southwest to northeast of the zero–wind stress curl line is reproduced. The surface heat flux Q_r is parameterized using the formula

$$Q_r = C_0(T_s - T_a), \quad (1)$$

where C_0 is a constant equal to 14.5 W m^{-2} K^{-1}, T_s is the SST, and T_a is an atmospheric temperature (Fig. 1c), which varies from 26°C at the equator to 2°C at the northwestern corner of the basin and includes a slight tilt from south west to north east in the midlatitudes. This forcing leads to a satisfactory mean oceanic circulation with a meridional overturning reaching 16 Sv (1 Sv ≡ 10^6 m^3 s^{-1}; Fig. 2a). South of 45°N, the gross features of the ocean circulation are reasonably reproduced, with a well-formed thermocline in the upper 700 m (Fig. 2b) and an intense subtropical gyre closed at the western boundary by a current of 35 Sv. On the other hand, the subpolar gyre is too confined in the northwestern part of the basin (Fig. 2c).

The heat flux Q_d, diagnosed at the end of the 540-yr period, is shown in Fig. 3. As expected, the maximum of intensity is over the northwestern boundary current, where it peaks at −60 W m^{-2}. This heat flux will be used in all the experiments described below as the mean heat flux forcing.

The reference state is used as an initial state for four experiments integrated for 200 yr with stochastic forcing

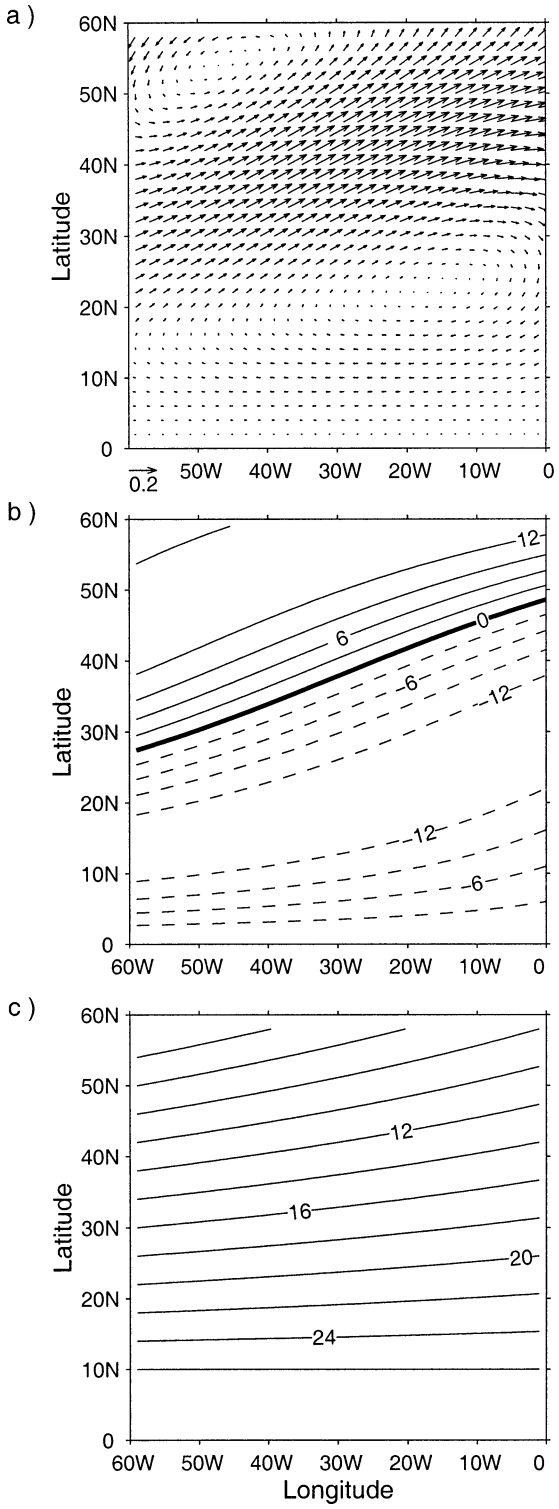

FIG. 1. (a) Mean wind stress (N m^{-2}), (b) Ekman pumping associated with the mean wind stress (10^{-7} m s^{-1}), and (c) temperature of the atmosphere (°C).

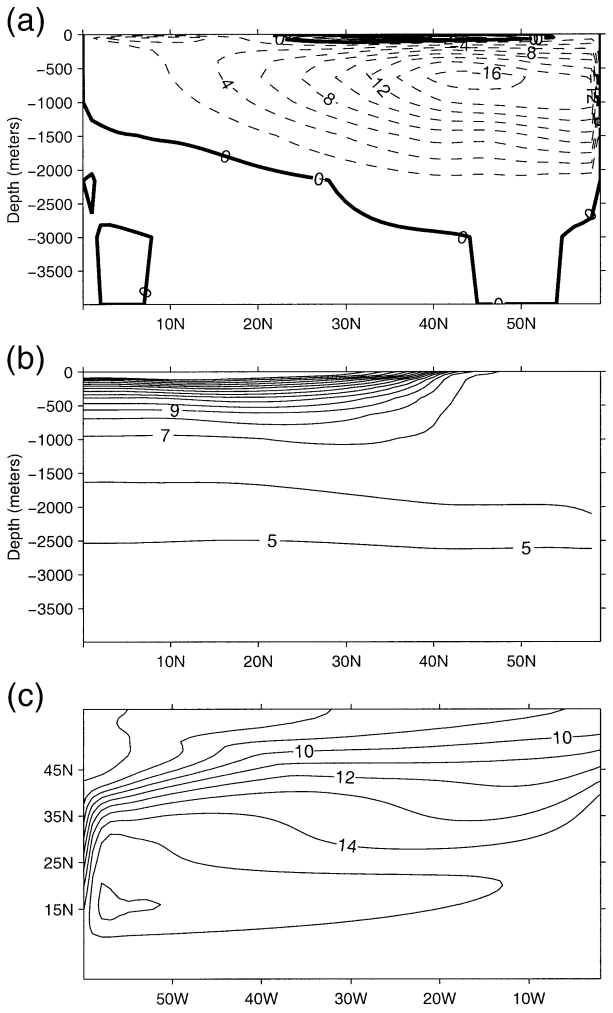

FIG. 2. (a) Meridional streamfunction (Sv), (b) north–south section of temperature [contour interval (CI) 1°C] along the western boundary, and (c) temperature at 300 m (CI 1°C) in the reference state.

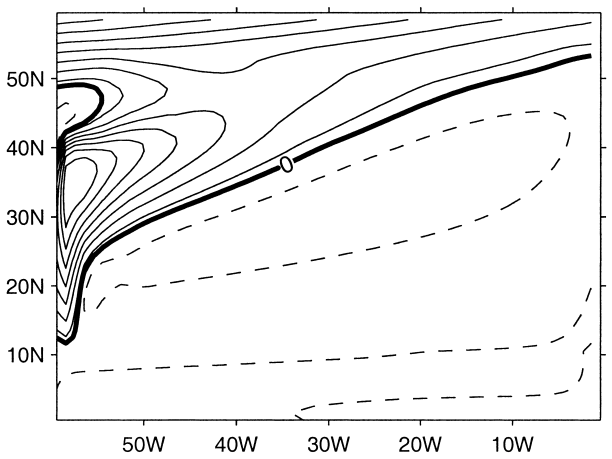

FIG. 3. Diagnosed surface heat flux Q_d at the end of the spinup (CI 20 W m^{-2}). Negative values (dashed contours) correspond to a heat loss for the atmosphere.

and one experiment integrated for 50 yr with deterministic forcing (Table 1). In the main experiment W_{st}—discussed in section 3—the ocean is forced by a stochastic NAO-like wind stress anomaly $W_a f(t_i)$ added to the constant wind stress W_r used during the spinup and by a constant thermal forcing equal to Q_d (the surface heat flux diagnosed at the end of the spinup). The spatial pattern W_a (Figs. 4a,b) mimics a wind stress anomaly field of high-NAO periods (cf. Fig. 1 in Marshall et al. 2001). The associated Ekman pumping anomaly is centered around 40°N where the curl of the wind stress W_r weakens (cf. Fig. 1b). The random discrete time series $f(t_i)$ has a 1-h sampling (which corresponds to the time step of the model) and has been built using a first-order autoregressive process with an autocorrelation timescale of 10 days. This timescale corresponds to the estimation by Feldstein (2000), using daily data from the NCEP–NCAR reanalysis. The variance of this series has been adjusted so that the time series built from the monthly means of the $f(t_i)$ has a variance equal to 1.

3. Existence of an oscillation excited by the wind

To characterize the overall response of the model in experiment W_{st}, we first made an analysis in empirical orthogonal functions (EOFs) and principal components (PCs) of the SST and temperature at 300 m (hereinafter T_{300}).

a. Decadal variability of temperature

Figure 5 shows the first two EOFs and PCs of the SST (Figs. 5a,b) and T_{300} (Figs. 5c,d). They represent approximatively 80% of the variance of the signal in both cases and show a temporal behavior that is similar. The autocorrelations of the different PCs show significant peaks at a 22–24-yr period, indicating an oscillatory behavior, even if the PCs of the SST are more noisy than those of T_{300}. Note that the cross correlation

TABLE 1. The numerical experiments.

Expt	Heat flux	Wind	Other characteristics	Length (yr)
W_{st}	Q_d	$W_r + f(t)W_a$	None	200
W_{da}	Q_d	$W_r + f(t)W_a$	SST damping	200
W_{zo}	Q_d	$W_r + f(t)W_z$	W_z is the zonal mean of W_a	200
Q_{st}	$Q_d + f(t)Q_a$	W_r	None	200
W_{de}	Q_d	$W_r + g(t)W_a$	$g(t) = 0.3$	50

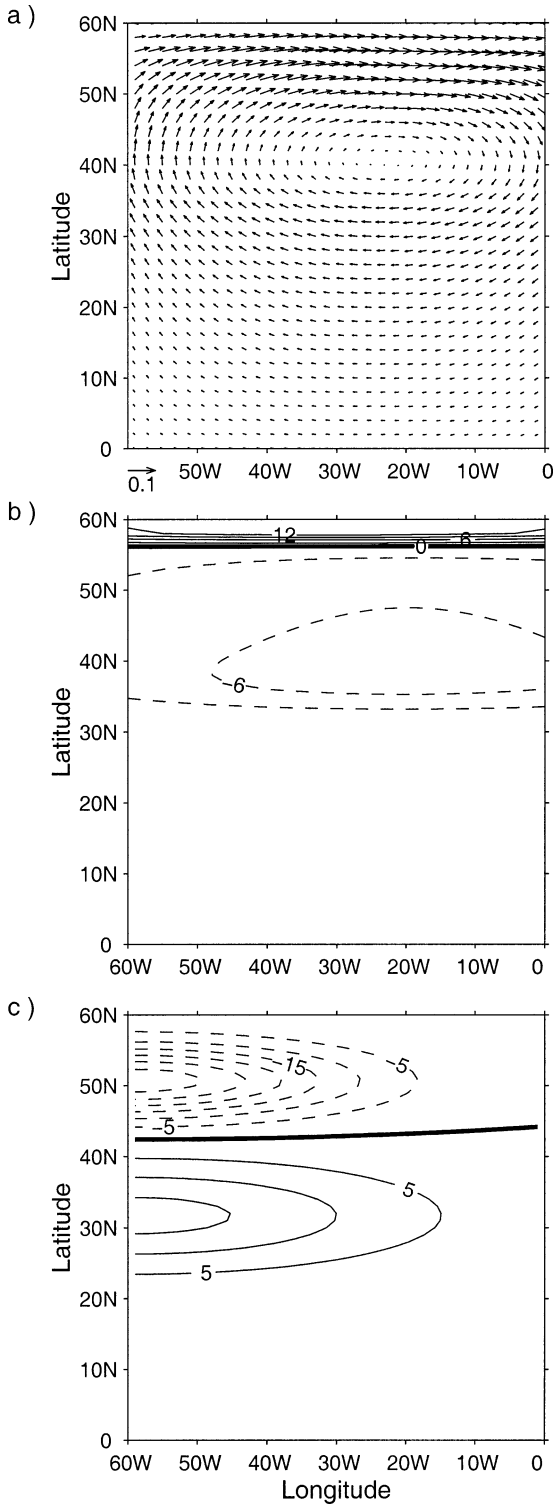

FIG. 4. (a) Wind stress anomaly W_a (N m^{-2}), (b) Ekman pumping anomaly (10^{-7} m s^{-1}), and (c) surface heat flux anomaly (W m^{-2}; only used in expt Q_{st}).

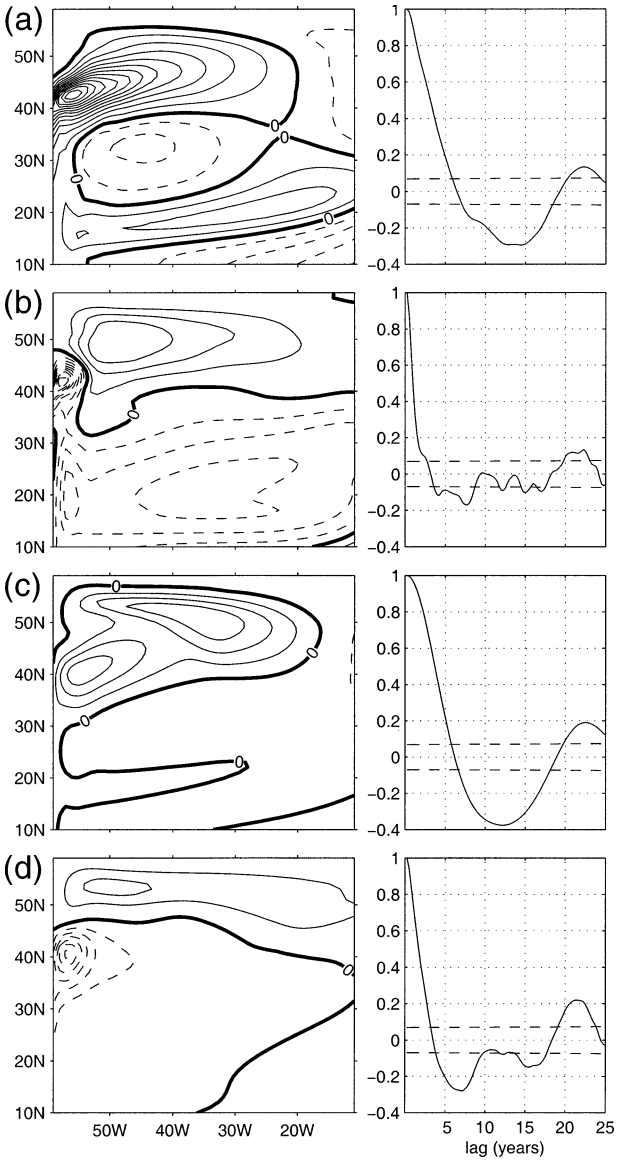

FIG. 5. (a), (b) First two (left) normalized EOFs and (right) autocorrelations of the corresponding PCs of the SST in expt W_{st} (CI 0.1°C); (c), (d) Same as (a) and (b) but for T_{300} (CI 0.1°C).

between the two PCs of T_{300} displays a strong negative peak when the second PC leads the first PC by 4 years (Fig. 6), suggesting that it takes around 4 years for a temperature anomaly to extend from the intergyre region into the subpolar gyre. On the other hand, the EOFs show large differences. The first EOF of SST is dominated by a positive anomaly slightly tilted northeastward, which extends north of 35°–40°N with a maximum near the western boundary around 42°N (Fig. 5a), whereas the first EOF of T_{300} shows two patterns of similar intensity, centered respectively at 40°N, 50°W and in the subpolar gyre at 50°N, 30°W. The second EOF of SST is characterized by a strong negative anomaly centered at 42°N along the western boundary, south-

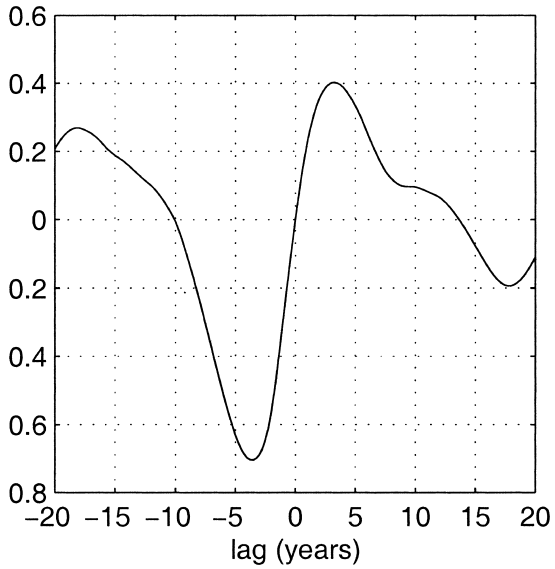

FIG. 6. Cross-correlation between the two PCs of T_{300}. The second PC leads for negative value.

westward of a larger but less intense positive anomaly. The second EOF of T_{300} has a similar strong negative anomaly, but the positive one is northward of it.

The regression of the SST onto the first PC of T_{300} (Fig. 7) shows at lag 0 a pattern that resembles the first EOF of SST. At lag +6 yr (SST follows), the positive SST anomaly persists only over the western part of the subpolar gyre while a cold anomaly develops in the intergyre region, progressively gains in intensity, and extends into the subpolar gyre. At lag +12 yr, the anomalies are similar to those at lag 0, but with an opposite sign and a weaker intensity. Afterward, the half cycle described above is repeated but with an opposite sign. During the cycle, the extrema of the SST anomalies are damped, reaching only −0.3°C at lag +12 yr, whereas they peaked at 1°C at lag 0.

The analysis of the oceanic heat transport allows us to understand how these temperature anomalies develop and ''propagate.'' Figure 8 shows, as a function of the time lag, the regression of the divergence of the heat transports at 300 m onto the first PC of T_{300}. This divergence is split into the gradient of temperature anomalies advected by the mean current $\overline{U} \cdot \nabla T'$ (dotted line) and the gradient of mean temperature advected by the anomalous currents $U' \cdot \nabla \overline{T}$ (solid line) in the intergyre region and in the western part of the subpolar gyre (the means are obtained by averaging over the 200 yr of integration). The term corresponding to the gradient of temperature anomalies advected by the anomalous currents is not shown because it is less important. Both panels show a damped oscillation with a 22–24-yr period. In the intergyre region, both terms are much stronger than in the subpolar gyre and they are out of phase, suggesting that the temperature anomalies generated by $U' \cdot \nabla \overline{T}$ are immediately advected by the mean current. In the western part of the subpolar gyre, $\overline{U} \cdot \nabla T'$ largely dominates.

These results suggest that the following mechanism is at play: in the intergyre region, where the forcing anomaly is the strongest, the response to the wind stress generates temperature anomalies through the advection of mean temperature by anomalous currents. The strongest temperature anomalies are located near the western boundary where the current anomalies and the mean temperature gradient are the most intense. These temperature anomalies are then advected by the northeastward mean current into the subpolar gyre.

b. Formation of a temperature anomaly in the intergyre region

The formation of intergyre temperature anomalies could be explained by the divergence of the heat transport caused by either the Ekman currents or by geostrophic currents induced by the wind stress curl anomaly. The regressions of the temperature at 80, 300, and 800 m onto the first PC of T_{300} (not shown) all have a similar anomaly pattern in the intergyre region. Because the divergence of the heat transport caused by Ekman currents affects mainly the surface layer and therefore would generate different responses in function of depth, the intergyre pattern cannot be produced by Ekman currents. Hence, below we will investigate only the second mechanism, briefly analyzing the forced and free responses of the isopycnals to the Ekman pumping variations.

A time–longitude diagram (not shown) of the 11° isotherm depth at 40°N does not show propagative patterns. Indeed, the variations of the isotherms around 40°N, between 10° and 45°W, are simply due to the forced Rossby waves excited by the strong wind stress anomalies that are applied at these latitudes (Herbaut et al. 2001). They lead to variations of the thermocline up to ±40 m. The response is large over the whole depth of the thermocline: a similar response is found for the 10° isotherm depth (near 800 m), suggesting that the first baroclinic mode is mainly excited. Near the western boundary (say, west of 50°W), the barotropic response to the wind stress dominates and helps to form the temperature anomalies described previously (Eden and Willebrand 2001; Herbaut et al. 2001).

c. Link between the SST variability and the overturning

Sections 3a and 3b mainly described the variability associated with the horizontal circulation. Below, we study whether the 22–24-yr oscillation has a component in the vertical and whether it is associated with the thermohaline circulation.

Figure 9 shows the regression of the meridional overturning streamfunction onto the first PC of T_{300}. At lag 0, there is a positive anomaly in the upper 500 m of the

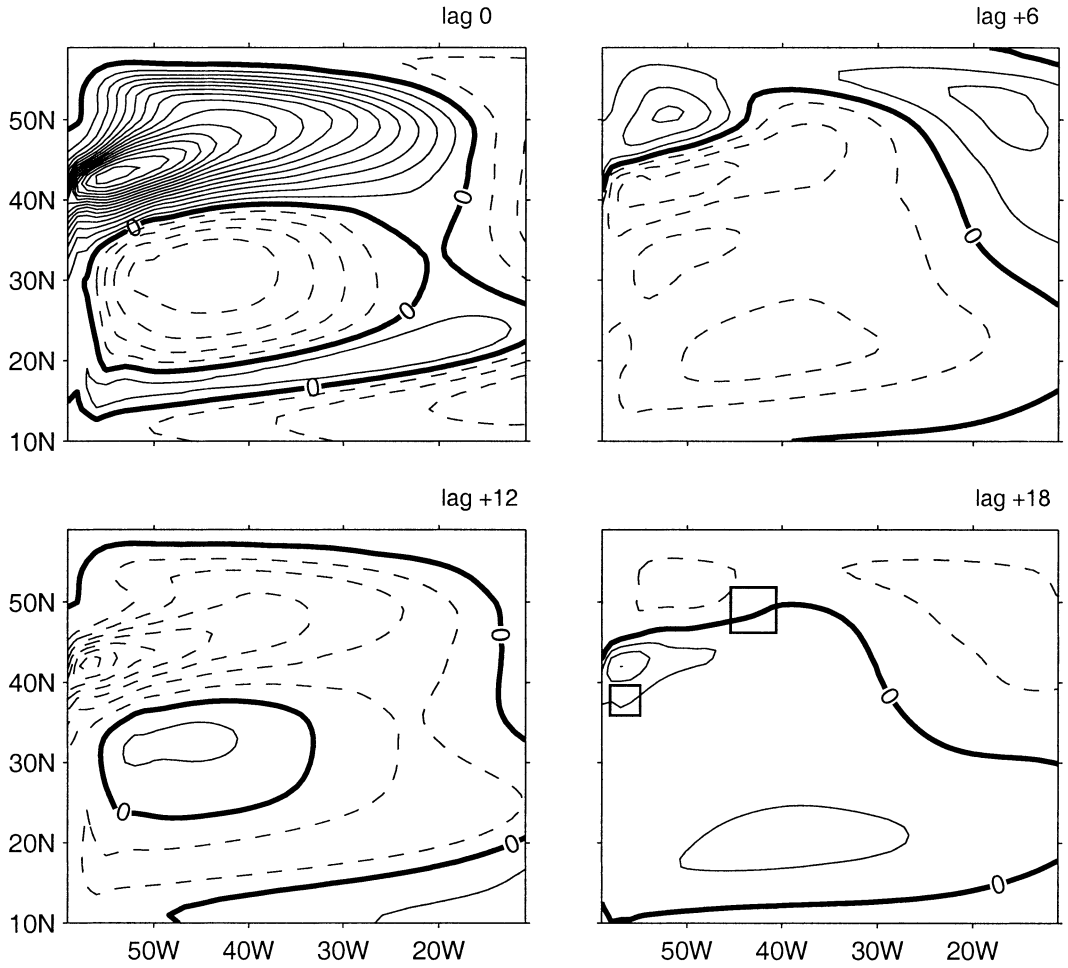

FIG. 7. Regression of the SST onto the first PC of T_{300} (CI 0.05°C; SST follows). The squares indicate the locations at which the heat transports shown in Fig. 8 are computed.

subpolar gyre and a much stronger negative anomaly below, reaching −0.5 Sv. The positive anomaly then expands to larger depths and gains in intensity. At lag +6 yr, it occupies the whole basin and peaks at 0.7 Sv near 45°N. At lag +12 yr (+18 years), an opposite pattern to the one obtained at lag 0 (+6 yr) has appeared, but its intensity has been largely reduced (e.g., at lag +18 yr, it peaks only at −0.3 Sv). Note that the amplitude of the overturning anomalies (about 0.7 Sv) represents only about 5% of the mean overturning. The evolution of the meridional overturning matches the evolution of the SST. Indeed, after lag 0, the convection is progressively inhibited because a positive SST anomaly is advected into the western part of the subpolar gyre (see the discussion of Figs. 5 and 7), contributing to the formation of a large positive meridional streamfunction anomaly by lag +6 yr. When negative SST anomalies are advected into the subpolar region, the stratification in the upper layers weakens, favoring convection and the development of a meridional streamfunction anomaly of opposite sign.

An EOF analysis of the meridional component of the velocity at different latitudes shows that the 22–24-yr oscillation is noticeable between 30°N and the northern boundary. However, the signal is more noisy at 40°N, because the direct response to the forcing is the strongest. Limiting this analysis to the band of longitude 60°–50°W and to the band 50°W–0° shows that the oscillation appears only in the boundary current between 30° and 40°N, whereas it extends over almost all the subpolar gyre.

In summary, the following picture emerges: temperature anomalies, forced in the intergyre region by the wind stress anomaly and advected into the subpolar gyre (see section 3a), modulate the overturning, which in turn drives a decadal variability of the western boundary current into the subtropical gyre.

4. Sensitivity experiments

In the previous section, we have shown that a coherent spatial pattern of wind stress excites an oscillation with

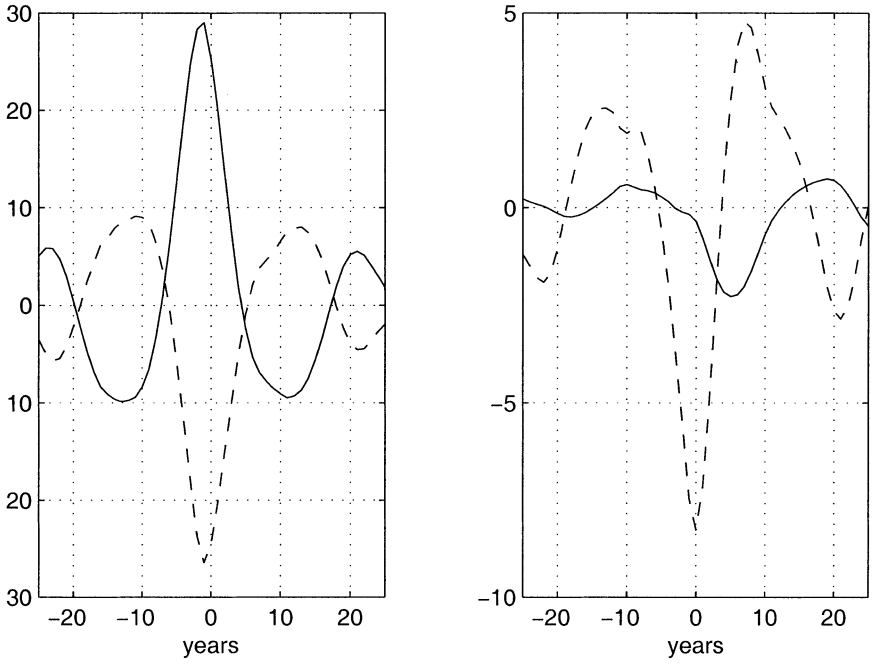

FIG. 8. Regression of $\overline{U} \cdot \nabla T'$ and $U' \cdot \nabla \overline{T}$ at 300 m onto the first PC of T_{300} (10^{-9} K s^{-1}) in the (left) intergyre region and (right) western part of the subpolar gyre. The solid line is for $U' \cdot \nabla \overline{T}$, and the dashed line is for $\overline{U} \cdot \nabla T'$. The heat transport terms follow for positive time.

a preferred 22–24-yr period. Even if part of the mechanism has been explained, we still ignore some of its properties. For example, does this oscillation still stand when an SST damping term is added? Does the timescale arise from the zonal length scale of the atmospheric forcing, as observed by Weng and Neelin (1998) in a forced model? If not, what sets up the timescale of the oscillation? Is it an advective ocean–atmosphere interaction similar to that described by Saravanan and McWilliams (1998), or is this oscillation a damped internal mode excited by a stochastic forcing as suggested by Griffies and Tziperman (1995) or Delworth and Greatbatch (2000) for the interdecadal oscillation of the Geophysical Fluid Dynamics Laboratory (GFDL) coupled model (Delworth et al. 1993)? Specific sensitivity studies will help to answer these questions.

a. Impact of an SST damping

In experiment W_{da}, the SST is restored toward the SST of the reference state with a constant *e*-folding time of 8 months. Note that this experiment is more realistic than the previous one in that it better represents the role of the atmosphere. An EOF analysis is performed onto the SST and T_{300}. The first two EOFs of SST (not shown) display similar patterns to those of W_{st} north of 25°N, but, south of 25°N, the anomalies are strongly damped; the EOFs of T_{300} slightly differ from those of W_{st}. However, the autocorrelations of the PCs are very similar to those of W_{st} and still suggest an oscillation at 22–24 yr, but the corresponding peaks are weaker. The regression of T_{300} onto its first PC (not shown) shows that the gross features of the evolution are the same as in W_{st} (temperature anomalies are generated in the western part of the intergyre region, then extend and propagate into the subpolar gyre), but with some temporal lags and an amplitude reduced by a factor of 2 or 3 at the half cycle. In conclusion, the SST damping damps the oscillation but cannot suppress it.

b. Impact of the zonal length scale of the forcing

Jin (1997) and Weng and Neelin (1998) suggested that a peak arises in the spectrum of the SST when the forcing has a specific zonal length scale. To determine whether their hypothesis could explain the oscillation observed in W_{st}, we carried out an experiment W_{zo} in which the wind stress anomaly W_a has been replaced by a zonal wind stress W_z. The latter is obtained by zonally averaging the zonal component of W_a and setting to 0 its meridional component. The first two EOFs of the SST and T_{300} are almost identical to those obtained in experiment W_{st}, and the autocorrelations of the PCs of T_{300} still display an oscillation with a 22–24-yr period. Thus, the oscillation observed in W_{st} does not originate in the zonal length scale of W_a. As suggested in section 3, the strong Ekman pumping anomaly in the intergyre region, independent of the details of its pattern, suffices to excite an oscillation in the ocean. Note that this oceanic oscillation might also be excited, but with a significantly weaker amplitude, by a ''white noise forcing both in space and time'' (Junge et al. 2000).

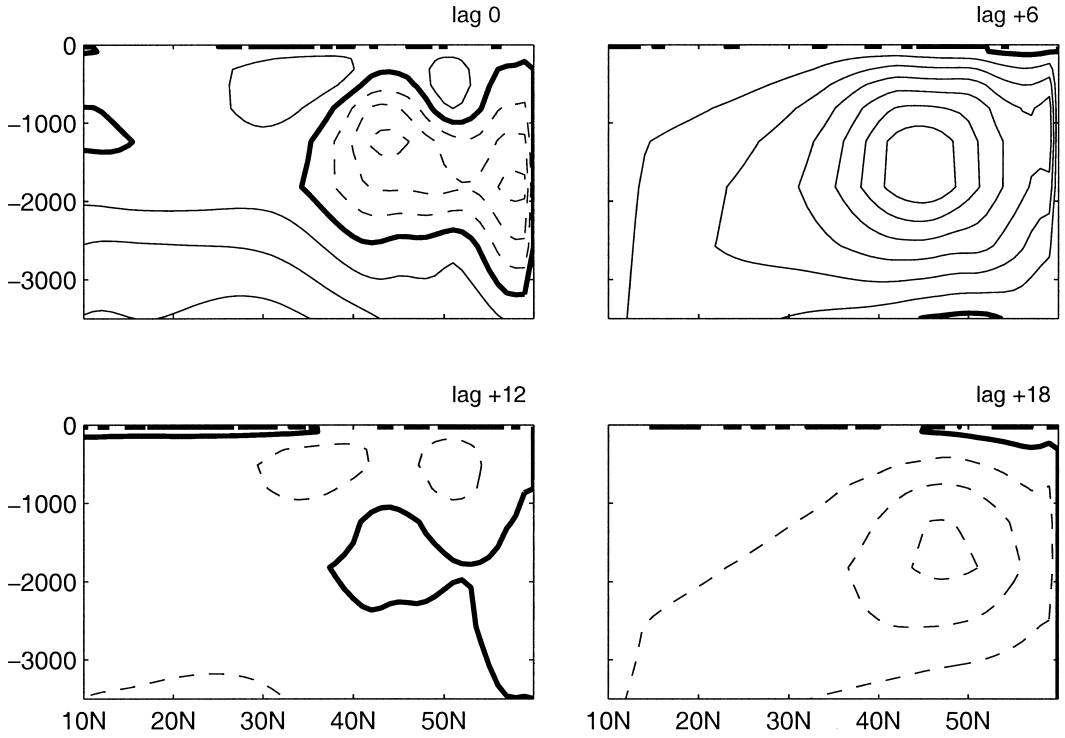

FIG. 9. Regression of the overturning streamfunction onto the first PC of T_{300} in expt W_{st} (CI 0.1 Sv). The overturning follows for positive time.

c. Evidence of the internal damped mode

Experiment W_{de} differs from the previous ones in that a deterministic forcing is used: the random series $f(t_i)$ is replaced by a constant series $g(t_i)$ equal to 0.3 (if the forcing is too strong the mean state is modified, and a comparison with W_{st} does not hold anymore). In box-geometry models forced by constant heat flux (Greatbatch and Zhang 1995; Colin de Verdière and Huck 1999) or by mixed boundary conditions (Weaver and Sarachik 1991), interdecadal unstable modes of the thermohaline circulation arise. Experiment W_{de} is carried out to establish whether the oscillation observed in W_{st} can be linked to such an internal mode.

The time evolution of the overturning clearly exhibits a 20-yr oscillation that is strongly damped (not shown). After 50 yr of integration, the model is close to equilibrium. The evolution of the SST anomalies over the first cycle of the oscillation (Fig. 10) is very similar to that described in experiment W_{st} (Fig. 7). This result suggests that the oscillation observed in W_{st} arises from a damped internal mode, which becomes sustained by the stochastic forcing in W_{st}. The strong damping of the oscillation in experiment W_{de} might be due to our choice of parameters: strong horizontal diffusion or weak vertical resolution (Huck et al. 1999).

d. Heat flux forcing contrasted with wind stress forcing

Experiment Q_{st} was carried out to determine whether NAO heat fluxes could excite the damped internal mode, and if so, how its amplitude compares with W_{st}. In consequence, in Q_{st}, the wind stress anomaly is set to 0 and Q_d is replaced by $Q_d + f(t_i)Q_a$, where Q_a mimics the heat flux anomaly of high-NAO periods. This heat flux anomaly is negative over the subpolar gyre and positive over the subtropical gyre, and its integral over the basin is null (Fig. 4c). Note that the time series is the same as in W_{st}. The analysis follows that of W_{st}.

The SST of experiment Q_{st} has been regressed onto the second PC of T_{300} of Q_{st} (Fig. 11). The regression shows SST anomalies propagating from the intergyre region into the subpolar basin, suggesting a dynamics similar to that observed in W_{st} (cf. Fig. 7). However, the amplitudes of the oscillations of SST and T_{300} are respectively divided by 5 and 3 in Q_{st}. As in W_{st}, the evolution of the streamfunction matches the evolution of the temperature in the upper layers: positive (negative) temperature anomaly in the western part of the subpolar gyre corresponds to the strongest positive (negative) meridional streamfunction anomaly (the regression of the meridional streamfunction displays the passage from a negative anomaly over the whole basin at lag 0 to a positive anomaly at lag +12). Moreover, the amplitudes of the oscillations in experiments W_{st} and Q_{st} are very similar.

This experiment suggests that stochastic heat or momentum flux anomalies can excite a similar internal mode. Both surface fluxes excite the oscillation of the overturning with comparable efficiency. However, sur-

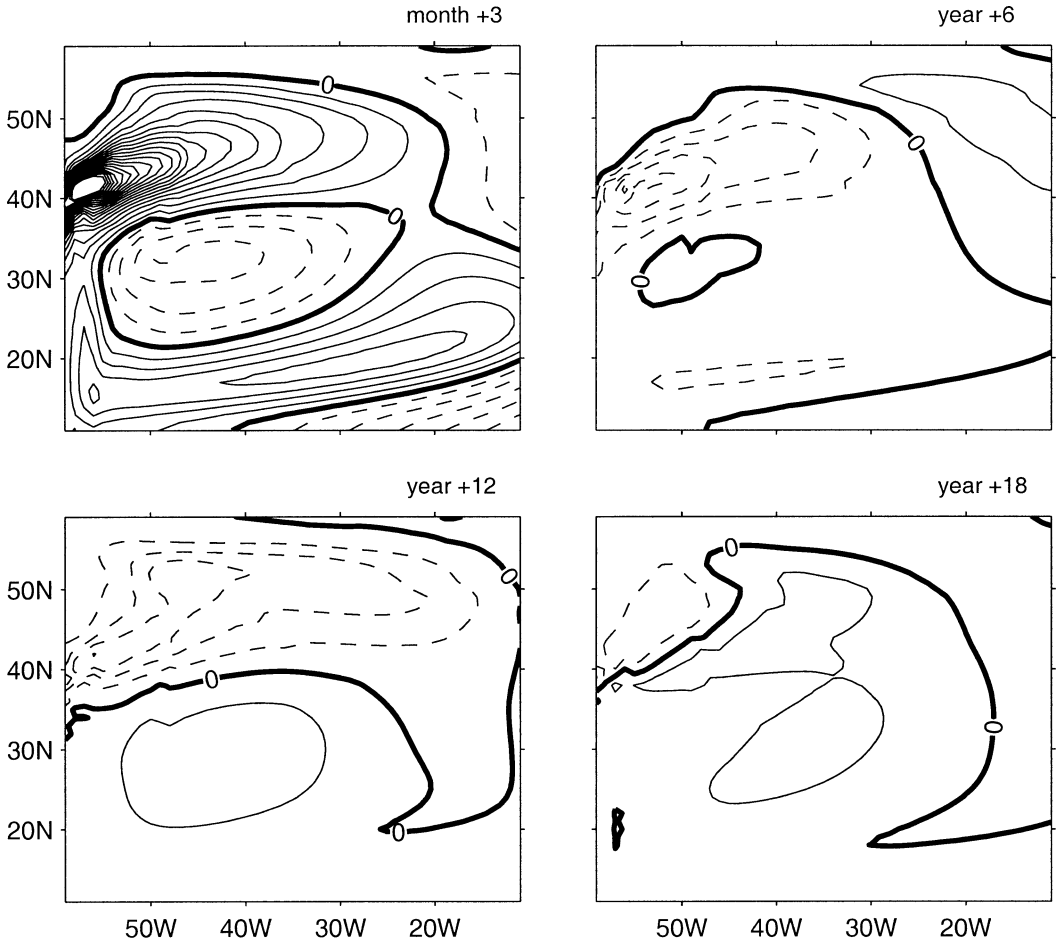

FIG. 10. Evolution of the SST in expt W_{de} (CI 0.1°C).

face and subsurface temperature anomalies related to the oscillation are much stronger in experiments with wind stress forcing.

5. Conclusions

A numerical experiment in which a simple oceanic GCM is driven by a wind stress that mimics the NAO variations has shown that the dominant response of the ocean is a damped internal mode of period 22–24 yr. Its mechanism is as follows. First, in response to wind stress forcing, anomalous currents appear between 35° and 40°N. Near the western boundary, the advection of the mean temperature by these current anomalies contributes to form temperature anomalies that are then advected by the mean current in the convection zone, inside the subpolar gyre. Because density is only a function of temperature, the temperature anomalies modify the thermohaline circulation, which in turn generates new temperature anomalies between 35° and 40°N. Because the mode is damped, a stochastic external forcing is needed to maintain the oscillation. As already pointed out by Marshall et al. (2001), these experiments emphasize the importance of the advection by anomalous currents generated by wind stress anomalies to excite the oscillation.

The mechanism described in this paper has strong similarities with those found by Saravanan et al. (2000) in an intermediate coupled model or by Delworth and Greatbatch (2000), who claimed that the interdecadal variability of the GFDL coupled model (Delworth et al. 1993) arises from a damped mode of the ocean system, excited by low-frequency atmospheric forcing. However, we found that momentum fluxes are as efficient as heat fluxes in exciting the oscillating mode, whereas in these previous papers heat fluxes have a prominent role. Note that the scaling used for the wind stress and heat flux anomalies is chosen to mimic observed NAO-related anomalies.

The period of the oscillation is shorter than that observed in the GFDL coupled model used by Delworth and Greatbatch (2000). Because the timescale is set by various processes (Rossby wave dynamics, advection by the mean flow, convection, etc.), it is difficult to give a single explanation for this difference. However, the mean state of our model has certainly a great impor-

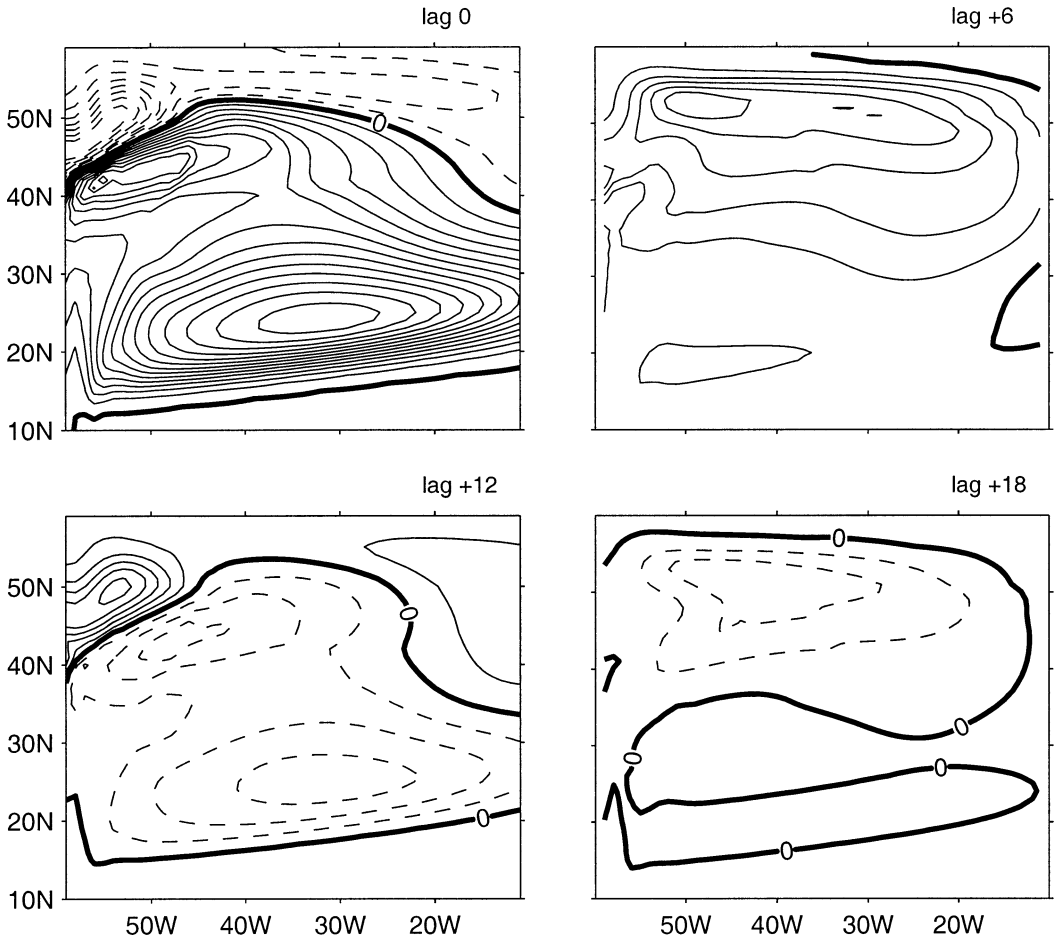

FIG. 11. Regression of the SST onto the second PC of T_{300} in expt Q_{st} (CI 0.02°C). The SST follows for positive time.

tance. Indeed the subpolar gyre is small in this model, and the time taken by the SST anomalies to reach the subpolar gyre from the intergyre region is thus short.

This study supports the Sutton and Allen (1997), Hansen and Bezdek (1996), and Krahmann et al. (2001) idea that SST anomaly can be formed off the east coast of North America and advected along the North Atlantic Current, as deduced from observations. However Krahmann et al. (2001) suggest that a similar mechanism to that proposed by Saravanan and McWilliams (1998) is at work in their model, whereas the oscillation described in this paper is associated with a damped thermohaline mode. The existence of a heat flux forcing anomaly with a dipolar pattern is necessary so that the Saravanan and McWilliams mechanism works. Although such an anomaly has been introduced in experiment Q_{st}, the response we observe remains close to that found in W_{st}. This result suggests that the mechanism found by Saravanan and McWilliams cannot explain the oscillation described here.

The strong current anomalies between the subpolar and subtropical gyres are induced by strong deepening of the mixed layer north of the current separating the gyres in our experiments. However, in the North Atlantic, the mixed layer north of the Gulf Stream and North Atlantic Current is shallow because surface salinity is weak (Levitus 1986). Adding salinity could therefore reduce the amplitude of the oscillation. Indeed, Greatbatch and Zhang (1995) show that salinity has an effect opposite to that of temperature on density anomalies but that decadal oscillations are just weakened in experiments with salinity. These authors also suggest that the oscillation of the GFDL coupled model is ''entirely thermally driven and that the role of salinity is to act as a brake.''

The setup of this model does not take into account topography and coastlines. Winton (1997) showed that bottom topography damps strongly unstable thermohaline modes, and Huck et al. (2001) revealed that the period of the oscillation is also very sensitive to the details of the topography. Bottom topography could also affect the oscillation by modifying the propagation of baroclinic Rossby waves and the transfer of energy to the barotropic mode (Tailleux and McWilliams 2000).

Acknowledgments. We thank G. Reverdin and C. Frankignoul for many fruitful discussions and comments on the manuscript. Comments by reviewers provided interesting suggestions and were helpful in improving the manuscript. Support from the European Union (EU Grant EVK2-CT-1999-00020, PREDICATE), is also gratefully acknowledged. Computations have been done at the Institut du Développement et des Ressources en Informatique Scientifique.

REFERENCES

Bryan, K., 1984: Accelerating the convergence to equilibrium of ocean–climate models. *J. Phys. Oceanogr.,* **14,** 666–673.

Cayan, D. R., 1992: Latent and sensible heat flux anomalies over the northern oceans: The connection to monthly atmospheric circulation. *J. Climate,* **5,** 354–369.

Colin de Verdière, A., and T. Huck, 1999: Baroclinic instability: An oceanic wavemaker for interdecadal variability. *J. Phys. Oceanogr.,* **29,** 893–910.

Cox, M. D., 1985: An eddy resolving numerical model of the ventilated thermocline. *J. Phys. Oceanogr.,* **15,** 1312–1324.

Delworth, T. L., and R. J. Greatbatch, 2000: Multidecadal thermohaline circulation variability driven by atmospheric surface flux forcing. *J. Climate,* **13,** 1481–1495.

——, S. Manabe, and R. J. Stouffer, 1993: Interdecadal variations of the thermohaline circulation in a coupled ocean–atmosphere model. *J. Climate,* **6,** 1993–2011.

Deser, C., and M. Blackmon, 1993: Surface climate variations over the North Atlantic Ocean during winter, 1900–1989. *J. Climate,* **6,** 1743–1753.

Eden, C., and J. Willebrand, 2001: Mechanism of interannual to decadal variability of the North Atlantic circulation. *J. Climate,* **14,** 2266–2280.

Feldstein, S. B., 2000: The timescale, power, and climate noise properties of teleconnection pattern. *J. Climate,* **13,** 4430–4440.

Frankignoul, C., P. Müller, and E. Zorita, 1997: A simple model of the decadal response of the ocean to stochastic wind stress forcing. *J. Phys. Oceanogr.,* **27,** 1533–1546.

Greatbatch, R. J., and S. Zhang, 1995: An interdecadal oscillation in an idealized ocean basin forced by constant heat flux. *J. Climate,* **8,** 81–91.

Griffies, S. M., and E. Tziperman, 1995: A linear thermohaline oscillator driven by stochastic atmospheric forcing. *J. Climate,* **8,** 2440–2453.

Grötzner, A., M. Latif, and T. P. Barnett, 1998: A decadal climate cycle in the North Atlantic Ocean as simulated by the ECHO coupled GCM. *J. Climate,* **11,** 831–847.

Hansen, D. V., and H. Bezdek, 1996: On the nature of decadal anomalies in North Atlantic sea surface temperature. *J. Geophys. Res.,* **101,** 8749–8758.

Herbaut, C., J. Sirven, and A. Czaja, 2001: An idealized model study of the mass and heat transports between the subpolar and subtropical gyres. *J. Phys. Oceanogr.,* **31,** 2903–2916.

Huck, T., A. Colin de Verdière, and A. J. Weaver, 1999: Interdecadal variability of the thermohaline circulation in box-ocean models forced by fixed surface fluxes. *J. Phys. Oceanogr.,* **29,** 865–892.

——, G. K. Vallis, and A. Colin de Verdière, 2001: On the robustness of the interdecadal modes of the thermohaline circulation. *J. Climate,* **14,** 940–963.

Jin, F. F., 1997: A theory of interdecadal climate variability of the North Pacific ocean–atmosphere system. *J. Climate,* **10,** 324–338.

Junge, M. M., J.-S. von Storch, and J. M. Oberhuber, 2000: Large-scale variability of the main thermocline excited by stochastic wind stress forcing. *J. Climate,* **13,** 2833–2840.

Krahmann, G., M. Visbeck, and G. Revedin, 2001: Formation and propagation of temperature anomalies along the North Atlantic Current. *J. Phys. Oceanogr.,* **31,** 1287–1303.

Kushnir, Y., 1994: Interdecadal variations in North Atlantic sea surface temperature and associated atmospheric conditions. *J. Climate,* **7,** 141–157.

Levitus, S., 1986: Annual cycle of salinity and salt storage in the world ocean. *J. Phys. Oceanogr.,* **16,** 322–343.

Marshall, J., A. Adcroft, C. Hill, L. Perelman, and C. Heisey, 1997: A finite-volume, incompressible Navier Stokes model for studies of the ocean on parallel computers. *J. Geophys. Res.,* **102,** 5753–5766.

——, H. Johnson, and J. Goodman, 2001: A study of the interaction of the North Atlantic oscillation with ocean circulation. *J. Climate,* **14,** 1399–1421.

Saravanan, R., and J. C. McWilliams, 1998: Advective ocean–atmosphere interaction: An analytical stochastic model with implications for decadal variability. *J. Climate,* **11,** 165–188.

——, G. Danabasoglu, S. C. Doney, and J. C. McWilliams, 2000: Decadal variability and predictability in the midlatitude ocean–atmosphere system. *J. Climate,* **13,** 1073–1097.

Sutton, R. T., and M. R. Allen, 1997: Decadal predictability of North Atlantic sea surface temperature and climate. *Nature,* **388,** 563–567.

Tailleux, R., and J. C. McWilliams, 2000: Acceleration, creation, and depletion of wind driven, baroclinic Rossby waves over an ocean ridge. *J. Phys. Oceanogr.,* **30,** 2186–2213.

Weaver, A. J., and E. S. Sarachik, 1991: Evidence for decadal variability in an ocean circulation model: An advective mechanism. *Atmos.–Ocean,* **29,** 197–231.

Weng, W., and J. D. Neelin, 1998: On the role of ocean–atmosphere interaction in midlatitude interdecadal variability. *Geophys. Res. Lett.,* **25,** 167–170.

Winton, M., 1997: The damping effect of bottom topography on internal decadal-scale oscillations of the thermohaline circulation. *J. Phys. Oceanogr.,* **27,** 203–208.